From the circular cylinder to the flat plate wake: The variation of Strouhal number with Reynolds number for elliptical cylinders

Alexander Radi, Mark C. Thompson, John Sheridan, and Kerry Hourigan

Citation: Physics of Fluids (1994-present) **25**, 101706 (2013); doi: 10.1063/1.4827521
View online: http://dx.doi.org/10.1063/1.4827521
View Table of Contents: http://scitation.aip.org/content/aip/journal/pof2/25/10?ver=pdfcov
Published by the AIP Publishing

PHYSICS OF FLUIDS **25**, 101706 (2013)

From the circular cylinder to the flat plate wake: The variation of Strouhal number with Reynolds number for elliptical cylinders

Alexander Radi,[1] Mark C. Thompson,[1,a)] John Sheridan,[1,b)] and Kerry Hourigan[1,2,c)]
[1]*Fluids Laboratory for Aeronautical and Industrial Research (FLAIR), Monash University, VIC 3800, Australia*
[2]*Division of Biological Engineering, Monash University, VIC 3800, Australia*

(Received 14 June 2013; accepted 16 October 2013; published online 30 October 2013)

The variation of Strouhal number with Reynolds number is quantified experimentally for a series of elliptical cylinders spanning aspect ratios between $Ar = 1$, corresponding to a circular cylinder, and $Ar = 0$, corresponding to a flat plate, over the Reynolds number range $100 \leqslant Re \leqslant 300$. The widths of the spectral peaks in Fourier space at each Reynolds number, together with changes in the shape or continuity of the Strouhal number curves, provide information of underlying three-dimensional transitions. Whilst modified versions of the mode A and B transitions of a circular cylinder wake occur at aspect ratios above $Ar \approx 0.4$, one major difference is observed for $Ar \lesssim 0.4$. In a limited range of Reynolds numbers, the wake appears to re-laminarize after it has already undergone three-dimensional transition. This flow regime is characterized by a strictly periodic vortex shedding. © *2013 AIP Publishing LLC*. [http://dx.doi.org/10.1063/1.4827521]

In the research of bluff body aerodynamics, several cross-sectional shapes have been used preferentially to study the flow about nominally two-dimensional bodies. Among these are the circular cylinder, the square or rectangular cylinders, the normal flat plate, and the 90° wedge.[1] Most studies treat these shapes separately, examining their unique flow properties. When comparing existing literature from a broad perspective, it is often difficult to identify flow phenomena shared by different body shapes, or in the case of absence of such similarities, to identify the body features causing the differences.

Adopting this broad view, we investigate the wake characteristics shared by a circular cylinder and a flat plate aligned normal to the flow. The link between these two models is formed by cylinders of elliptical cross sections of varying aspect ratios Ar. We define Ar as the ratio of the minor to major ellipse axes; with $Ar = 1.00$ corresponding to the circular cylinder and $Ar = 0$ being the flat plate (compare Figure 1(b)).

This article discusses changes to the Strouhal–Reynolds number relationship (*St–Re* curves) as a function of the aspect ratio Ar in the range $100 < Re < 300$. The non-dimensional parameters are defined as $St = fd/U$ (f: shedding frequency; d: main cylinder diameter; and U: freestream velocity), and $Re = dU/\nu$ (d, U as before; ν: kinematic viscosity of the fluid).

For the circular cylinder, the Strouhal numbers lie on a curve that has been established by many experimental (e.g., Williamson[2] and references therein) and numerical (e.g., Henderson[3]) studies. For this model, the *St–Re* curve reflects the major flow regimes and transitions of the wake, in the form of possibly hysteretic discontinuities and slope changes.[4] We attempt to use this "imprint" of

a)Mark.Thompson@monash.edu
b)John.Sheridan@monash.edu
c)Kerry.Hourigan@monash.edu

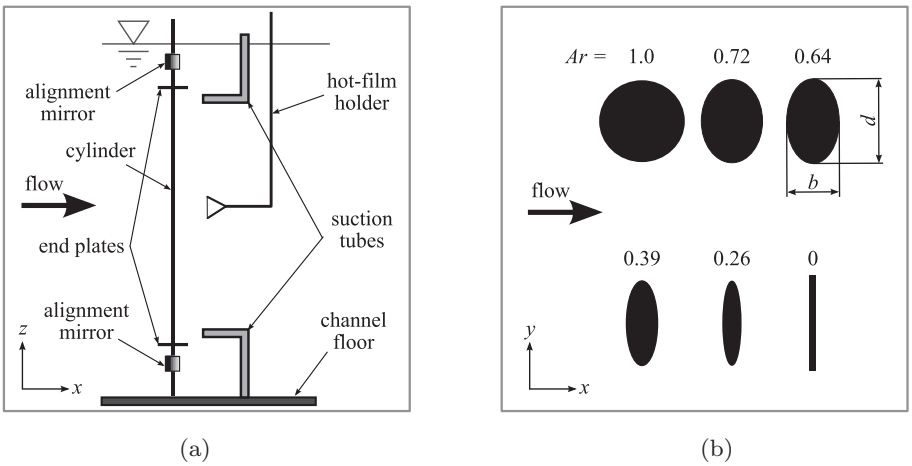

FIG. 1. (a) Schematic of the experimental setup from a side perspective. (b) Cross-sections of the cylinder models and their orientation to the incoming flow.

a cylinder's wake transition behaviour as a guide in the search for wake transitions of other, less studied, cylinder types.

This approach is very promising when studying the largely unexplored elliptical cross-section cylinders. In most previous investigations, this model type has been studied either at very high Reynolds numbers[5–7] or under Stokes flow conditions.[8] In the majority of cases, the main axis of the ellipse is aligned in the streamwise direction, or at an angle of attack $\neq 90^\circ$. The critical Reynolds numbers Re_{c_0} for the onset of vortex shedding are known to decrease for smaller aspect ratios.[9] Several Strouhal numbers have been reported for an $Ar = 0.25$ cylinder using two-dimensional numerical simulations.[10] Apart from this knowledge, no further literature could be found on the shape of the *St–Re* curves or the existence of three-dimensional modes for the proposed Reynolds number range and cylinder orientation.

The present study seeks to obtain these curves, identify associated flow transitions and their potential causes, and to compare the transition scenarios of the elliptical cylinders to the two limiting cases of a flat plate and circular cylinder.

The experimental setup is shown in Figure 1(a). The cylinders were mounted vertically in an open surface water channel, having a freestream turbulence of 0.5%–1%. The usable model length ($100d$) was defined by circular end plates of $10d$ diameter, oriented parallel to the flow. To induce parallel shedding, suction tubes[4,11] were installed downstream of and close to the end plates. The flow rate of each tube was monitored by a flow meter and adjusted until parallel shedding was confirmed by flow visualizations.

Figure 1(b) shows the model cross-sections ($d = 6$ mm). The elliptical cylinders were printed in a rapid prototyping process from Accura Xtreme plastic with an engineering finish (bead-blast); a carbon fibre tube was used as the circular cylinder; and the flat plate model was a thin brass strip with sharp untapered edges (7% plate thickness). The main axis of the elliptical cross section was aligned perpendicular to the flow using an optical setup consisting of small mirrors glued to the cylinder ends and a laser beam (the flat plate was aligned in the same way). This technique allowed an uncertainty of alignment of $\pm 0.4^\circ$. To prevent vortex induced vibrations, the models were tensioned by a spring-loaded linear slide at the upper fix point.

A hot-film probe, placed at $(x, y) \approx (10d, -1.5d)$, was used to record the velocity fluctuations. The analogue signal was low-pass filtered at 10 Hz and sampled at 20 Hz. For each Reynolds number, a velocity time series of 20 min was recorded (equivalent to 440–1600 main shedding cycles). The Reynolds numbers were increased stepwise from 100 to 300; then the series was reversed, to capture any hysteretic effects in the flow. The water temperature was measured throughout the experiments, to correct for changes in viscosity. The freestream velocity was recorded simultaneously by a laser Doppler velocimeter (LDV) upstream of the model. The uncertainty of the Reynolds and Strouhal

numbers was ±3% at a confidence level of 95% (for $Re = 200$). This value was dominated by the random error of the velocity measurement, due to the relatively high noise level of the LDV at such low velocities. Two error bar examples are shown in Figure 2(a) at $Re = 100$ and 300.

To obtain the shedding frequency, a windowed fast Fourier transform (FFT) was performed on the velocity time series, with a window width of 512 points (25.3 s), and 50% overlap. The spectra of all windows were averaged and the highest peak identified as the Bénard-von Kármán shedding frequency. The width of the frequency peak in the power spectrum contains useful information on the transition process.[2] This *spectral bandwidth* Δf^* is defined as the difference between the frequencies where the spectral level is 3 dB below the peak in the spectrum.[12] As the results depend on the used window width, only relative values will be given. All values of Δf^* are normalized with the averaged spectral bandwidth of the circular cylinder in the laminar regime ($Re < 177$ in our experiments).

The hydrogen bubble technique was used for flow visualizations. A 50 μm platinum wire, 500 mm long, was soldered between the prongs of an F-shaped stainless steel frame and aligned parallel to the cylinder. The wire could be moved in the x–y plane by a two-axes traverse. A continuous laser sheet, aligned parallel to the x–z plane, was used to illuminate the flow structures. Pictures were taken from a side perspective with a digital camera, from which the modes' spanwise wavelengths were estimated.

To make all three-dimensional transitions associated with the different cylinder types more comparable, the following terminology will be used for the three-dimensional modes: (1) "Mode L" refers to a long-wavelength instability appearing at lower Reynolds numbers. This is equivalent to mode A for the circular cylinder. (2) "Mode S" refers to a short-wavelength instability (similarly equivalent to mode B) at higher Re. Their critical Reynolds numbers are Re_{c_1} and Re_{c_2}; λ_L, λ_S are the wavelengths of each mode. Note that for larger aspect ratios the identified modes are effectively equivalent to variants of modes A and B; however, for lower aspect ratios, and especially the flat plate, they do not necessarily correspond to the circular cylinder modes. This aspect will be investigated in detail in future studies.

The validation of our setup is presented in Figure 2(a), which shows the *St–Re* curve for the circular cylinder. The initial section of the curve is known to begin outside of the measured Reynolds number range at $Re_{c_0} \approx 47$, when the steady wake starts shedding spanwise vortices of alternate sign.[4,14,15] The Strouhal numbers increase monotonously until a hysteretic discontinuity at $Re_{c_1} = 160$–190 (depending on the experimental conditions[4]). The discontinuity is reproduced accurately in our experiment at $Re = 177$ with a pronounced hysteresis. This sudden drop is caused by the appearance of the first three-dimensional mode (mode A) with a spanwise wavelength $\lambda_L = 3$–4,[16,17] combined with large-scale vortex dislocations, which evolve spontaneously and intermittently along the span. These dislocations lead to low-frequency irregularities of the measured velocity signal and to a broadening of the spectral bandwidth, which is the reason for the first sharp peak in the Δf^* curve at $Re \approx 180$. For Reynolds numbers above 220, perturbation energy is gradually transferred to the second three-dimensional mode (mode B) with $\lambda_S \approx 1$,[16–19] which dominates the wake completely at $Re = 260$.[4] During this gradual transition, the *St–Re* curve experiences a steep increase, followed by a plateau; the Δf^* curve exhibits a broader peak centred at $Re = 230$. The *St–Re* curve plateaus in our experiments at $Re > 250$, with a dimensionless shedding frequency of $St_{300} \approx 0.20$ measured at $Re = 300$.

Figure 2(b) shows the *St–Re* curve and the spectral bandwidths of the $Ar = 0.72$ cylinder. The steep drop in Strouhal number is the most prominent feature of this curve. The following changes compared to the circular cylinder are observed: (1) The discontinuity, which is again caused by the appearance of a three-dimensional mode with $\lambda_L = 3.7$–4.0, is shifted to a lower critical Reynolds number $Re_{c_1} = 135$. (2) The steep increase of Strouhal numbers, associated with the circular cylinder's mode B, is not present. Yet, flow visualizations confirm the presence of a short-wavelength mode with $\lambda_S \approx 1.3$ for $Re > 160$–190 (not shown). (3) The *St–Re* curve plateaus at a lower value of $St_{300} \approx 0.19$. Overall, the curve for the $Ar = 0.72$ cylinder appears to be just a modified version of the circular cylinder's curve. The same observation holds for the $Ar = 0.64$ cylinder (Figure 2(c)). Only for smaller aspect ratios below $Ar = 0.39$ are major changes observed, which are indicative of new physical processes.

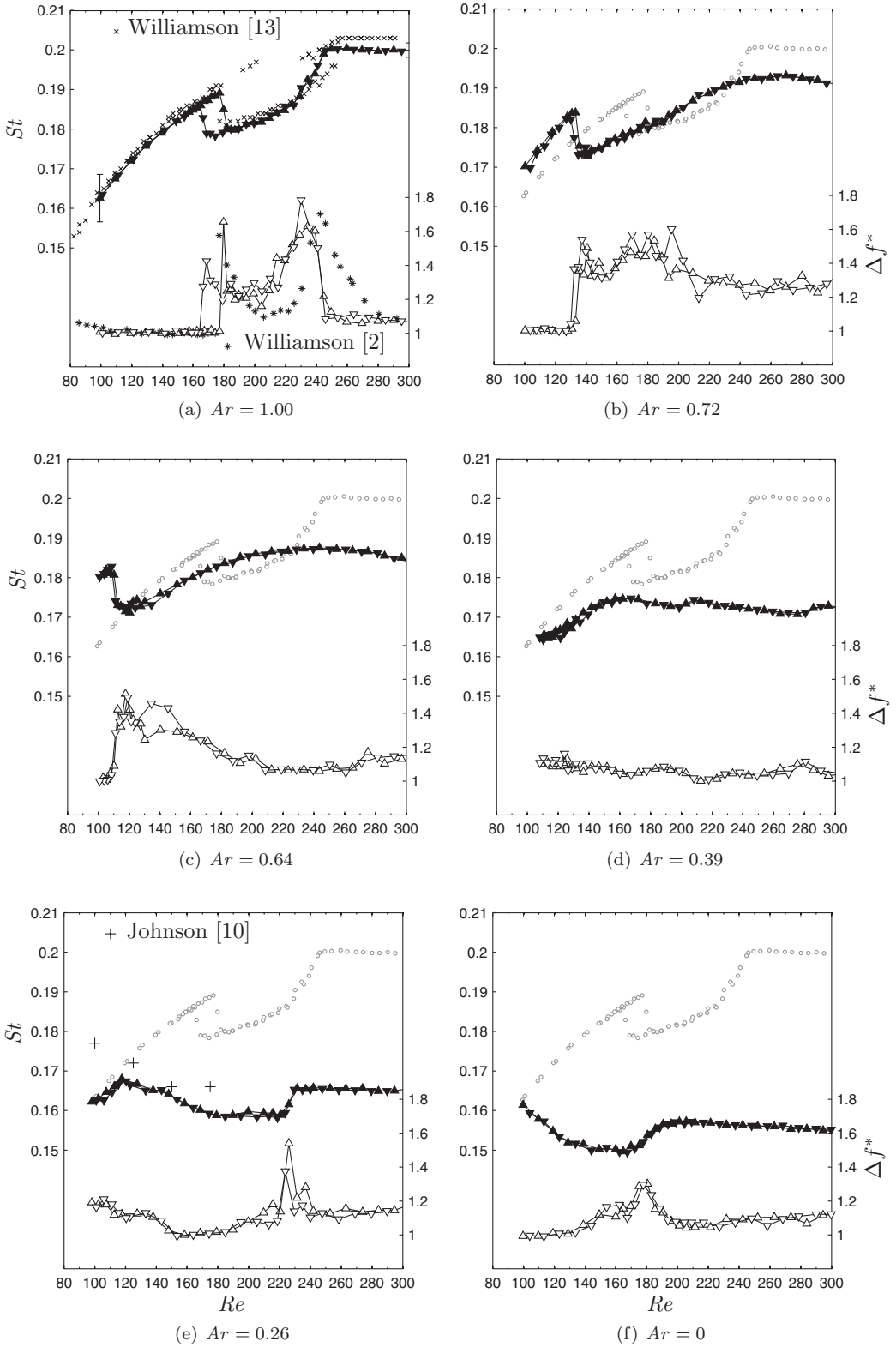

FIG. 2. *St–Re* curves and spectral bandwidths of all cylinder models (filled and empty triangles). The Reynolds number has been increased (triangles up), and then decreased (triangles down) to capture hysteresis effects. The curve of the circular cylinder ($Ar = 1.00$) is reproduced in each plot for easier comparison (gray circular symbols). Literature data[2,10,13] are shown for comparison as line symbols (cross, star, plus); data by Williamson[2] are rescaled and normalized.

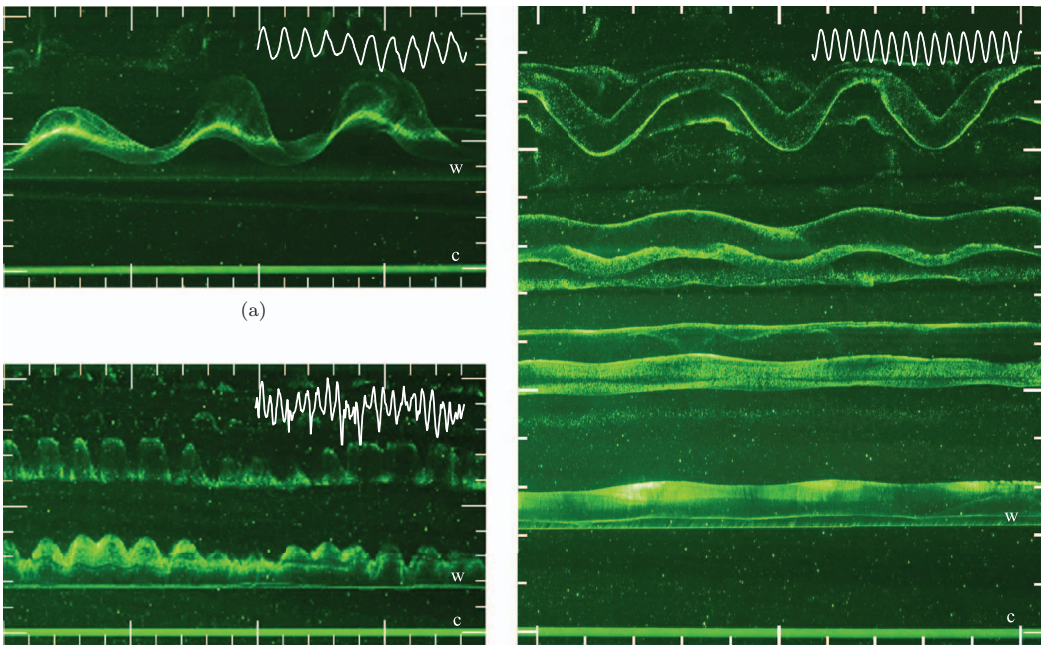

FIG. 3. Flow visualizations of the $Ar = 0.26$ cylinder wake. (a) $Re = 100$: mode L with $\lambda_L \approx 6d$; (b) $Re = 200$: mode S with $\lambda_S \approx 1.4d$; and (c) $Re = 160$: re-laminarized wake. The insets in the top right corners show typical hot-film signals (measured at $x/d \approx 10$). The ticks along the picture frame are $1d$ apart. The cylinder and hydrogen bubble wire are marked by "c" and "w," respectively. The flow is from bottom to top.

These changes will be highlighted with results for the $Ar = 0.26$ cylinder, with its *St–Re* curve shown in Figure 2(e). This curve differs fundamentally from that for the circular cylinder. First, it must be emphasized that the Strouhal number drop at $Re \approx 120$ is *not* the discontinuity marking the transition to three-dimensional flow. This transition takes place outside of the measured range at $Re < 100$, with the flow already being fully three-dimensional with a mode L structure at the lowest Reynolds numbers investigated. Accordingly, the spectral bandwidths are large in the range $100 < Re < 150$, and the hot-film signals show low-frequency irregularities, reminiscent of mode A and vortex dislocations known to occur from the circular cylinder.

In addition to the strongly decreased critical Reynolds number Re_{c_1}, two more unique properties are noticed: (1) A steep increase of the Strouhal numbers at $Re \approx 225$, accompanied by a peak in the spectral bandwidth. (2) A gradual decrease of Strouhal numbers over the range $120 < Re < 180$, paired with the lowest spectral bandwidths measured for this cylinder type between $150 < Re < 190$.

The steep increase of the Strouhal numbers at $Re \approx 225$ can be reliably attributed to the appearance of the three-dimensional mode S. At this Reynolds number, this short-wavelength mode is fully developed with a wavelength of $\lambda_S = 1.4d$. This mode appears intermittently already at $Re = 200$ (Figure 3(b)), which explains the increased spectral bandwidths.

For $Re < 150$, flow visualizations show the long-wavelength mode L, having a wavelength $\lambda_L \approx 5d$ (Figure 3(a)). This mode strongly deforms the Bénard-von Kármán vortices from their inception. The presence of a three-dimensional mode is the most likely reason for the differences between Strouhal numbers obtained by Johnson[10] in two-dimensional computations and the present study (compare Figure 2(e), particularly $Re < 120$). Surprisingly, this discrepancy decreases as the Reynolds number approaches 150. The decrease of *St* is caused by a change of the flow behaviour in the experiment: the near wake becomes two-dimensional again in the range $150 < Re < 190$, void of three-dimensional modes or vortex dislocations! Figure 3(c) shows that during this regime, the Bénard-von Kármán vortex cores are shed initially parallel to the cylinder axis, with only a

TABLE I. Overview of all investigated models. Missing data were linearly interpolated from results by Jackson.[9] (H) denotes hysteretic transitions.

Ar	Re_{c_0}	Re_{c_1}	Re_{c_2}	λ_L	λ_S	St_{300}	Re-laminarization
1.00	45.4[9]	177 (H)	220–260	3.96[23]	0.822[23]	0.20	No
0.72	40.1[9]	135 (H)	160–190	3.7–4.0	1.3	0.191	No
0.64	38.2[9]	110	140–160	4–6	1.2–1.4	0.184	No
0.39	34.2[9]	<100	220	4–6	1.1–1.2	0.172	Weak
0.26	32.0[9]	<100	220–230	5–6	1.4	0.165	Yes
0	27.8[9]	N/A	180–200	N/A	1.4	0.155	Yes

minor spanwise modulation. This modulation is amplified strongly as the vortex cores are advected downstream, which is indicative of a high strain region for distances $10 \lesssim x/d$.

This new flow regime will be referred to as "re-laminarized," because it is characterized by a strictly periodic hot-film signal and narrow spectral bandwidths, which is similar to the laminar shedding regime of the circular cylinder at $Re \lesssim 190$ (no reference is made by this term to the distinction between laminar and turbulent flows!). A comparison of hot-film traces in Figure 3 exemplifies this trend. The velocity signal in (a), prior to re-laminarization, shows gradual amplitude modulations, which are characteristic of vortex dislocations. Once mode S appears, the velocity signal in (b) exhibits high frequency bursts. During the new regime, the velocity trace is strictly periodic with a constant amplitude, as seen in (c).

Currently, it is not clear what mechanism is responsible for the re-laminarized regime, but it is suspected that a fundamental change of the underlying base flow takes place, stabilising the wake with respect to three-dimensional disturbances. Apart from the $Ar = 0.26$ cylinder, this newly found regime was observed in a weaker form in the $Ar = 0.39$ wake for $200 < Re < 250$, although its St–Re curve does not show such a pronounced decrease of Strouhal number (Figure 2(d)).

The St–Re curve of the flat plate resembles the $Ar = 0.26$ curve, with the transitions shifted to lower Reynolds and Strouhal numbers (Figure 2(f)), tempting the interpretation of its features in the same way. The steep increase of St values between $Re = 170$ and 200 is indeed accompanied by the appearance of a short-wavelength mode S, which is fully developed at $Re > 200$ with a wavelength $\lambda_S \approx 1.4$. This is in accordance with reports of a short-wavelength mode for $Re > 200$.[20,21] The steep decrease of Strouhal numbers at $Re < 160$ resembles the curve behaviour of the new re-laminarized regime. Yet, flow-visualizations did not show conclusively the absence of a long-wavelength mode. Further studies of the flat plate in this Reynolds number range are needed, in particular those regarding evidence of long-wavelength instabilities in simulations.[22]

The main experimental observations are summarized in Table I.

[1] J. F. Foss, C. Tropea, and A. L. Yarin, *Springer Handbook of Experimental Fluid Mechanics* (Springer Science+Business Media, Berlin, 2007).
[2] C. H. K. Williamson, "Three-dimensional wake transition," J. Fluid Mech. **328**, 345–407 (1996).
[3] R. Henderson, "Nonlinear dynamics and pattern formation in turbulent wake transition," J. Fluid Mech. **352**, 65–112 (1997).
[4] C. H. K. Williamson, "Vortex dynamics in the cylinder wake," Annu. Rev. Fluid Mech. **28**, 477–539 (1996).
[5] V. J. Modi and E. Wiland, "Unsteady aerodynamics of stationary elliptic cylinders in subcritical flow," AIAA J. **8**, 1814–1821 (1970).
[6] V. J. Modi and A. K. Dikshit, "Near-wakes of elliptic cylinders in subcritical flow," AIAA J. **13**, 490–497 (1975).
[7] T. Ota, H. Nishiyama, and Y. Taoka, "Flow around an elliptic cylinder in the critical Reynolds number regime," J. Fluids Eng. **109**, 149–155 (1987).
[8] K. Shintani, A. Umemura, and A. Takano, "Low-reynolds-number flow past an elliptic cylinder," J. Fluid Mech. **136**, 277–289 (1983).
[9] C. P. Jackson, "A finite-element study of the onset of vortex shedding in flow past variously shaped bodies," J. Fluid Mech. **182**, 23–45 (1987).
[10] S. A. Johnson, M. C. Thompson, and K. Hourigan, "Predicted low frequency structures in the wake of elliptical cylinders," Eur. J. Mech. B/Fluids **23**, 229–239 (2004).
[11] G. D. Miller and C. H. K. Williamson, "Control of three-dimensional phase dynamics in a cylinder wake," Exp. Fluids **18**, 26–35 (1994).

[12] A. Prasad and C. H. K. Williamson, "Three-dimensional effects in turbulent bluff-body wakes," J. Fluid Mech. **343**, 235–265 (1997).
[13] C. H. K. Williamson, "The natural and forced formation of spot-like 'vortex dislocations' in the transition of a wake," J. Fluid Mech. **243**, 393–441 (1992).
[14] J. Dusek, P. Le Gal, and D. P. Fraunie, "A numerical and theoretical study of the first Hopf bifurcation in a cylinder wake," J. Fluid Mech. **264**, 59–80 (1994).
[15] P. Le Gal, A. Nadim, and M. C. Thompson, "Hysteresis in the forced Stuart-Landau equation: Application to vortex shedding from an oscillating cylinder," J. Fluids Struct. **15**, 445–457 (2001).
[16] C. H. K. Williamson, "The existence of two stages in the transition to three-dimensionality of a cylinder wake," Phys. Fluids **31**, 3165–3168 (1988).
[17] D. Barkley and R. D. Henderson, "Three-dimensional Floquet stability analysis of the wake of a circular cylinder," J. Fluid Mech. **322**, 215–241 (1996).
[18] J. Wu, J. Sheridan, M. C. Welsh, and K. Hourigan, "Three-dimensional vortex structures in a cylinder wake," J. Fluid Mech. **312**, 201–222 (1996).
[19] M. C. Thompson, K. Hourigan, and J. Sheridan, "Three-dimensional instabilities in the wake of a circular cylinder," Exp. Therm. Fluid Sci. **12**, 190–196 (1996).
[20] F. M. Najjar and S. P. Vanka, "Effects of intrinsic three-dimensionality on the drag characteristics of a normal flat plate," Phys. Fluids **7**, 2516 (1995).
[21] F. M. Najjar and S. Balachandar, "Low-frequency unsteadiness in the wake of a normal flat plate," J. Fluid Mech. **370**, 101–147 (1998).
[22] M. C. Thompson, K. Hourigan, K. Ryan, and G. J. Sheard, "Wake transition of two-dimensional cylinders and axisymmetric bluff bodies," J. Fluids Struct. **222**, 793–806 (2006).
[23] R. D. Henderson and D. Barkley, "Secondary instability in the wake of a circular cylinder," Phys. Fluids **8**, 1683–1685 (1996).